Mississippi State University
Scholars Junction

Honors Theses | Undergraduate Research

5-1-2019

Investigation of Radiation Effects on Tungsten and Numerical methods to Determine Indentation Modulus

Erin M. O'Quinn
Mississippi State University

Follow this and additional works at: https://scholarsjunction.msstate.edu/honorstheses

Recommended Citation

O'Quinn, Erin M., "Investigation of Radiation Effects on Tungsten and Numerical methods to Determine Indentation Modulus" (2019). *Honors Theses*. 43.
https://scholarsjunction.msstate.edu/honorstheses/43

This Honors Thesis is brought to you for free and open access by the Undergraduate Research at Scholars Junction. It has been accepted for inclusion in Honors Theses by an authorized administrator of Scholars Junction. For more information, please contact scholcomm@msstate.libanswers.com.

Investigation of Radiation Effects on Tungsten and Numerical Methods to Determine Indentation Modulus

By

Erin M. O'Quinn

A Thesis
Submitted to the Faculty of
Mississippi State University
in Partial Fulfillment of the Requirements
for the Degree of Bachelor of Science
in Mechanical Engineering
in the Department of Mechanical Engineering

Mississippi State, Mississippi

May 2019

Copyright by

Erin M. O’Quinn

2019

Name: Erin M. O'Quinn

Date of Degree: May 3, 2019

Institution: Mississippi State University

Major Field: Mechanical Engineering

Major Professor: Dr. Matthew W. Priddy

Title of Study: Investigation of Radiation Effects on Tungsten and Numerical Methods to Determine Indentation Modulus

Pages of Study: 34

Candidate for Degree of Bachelor of Science

The purpose of this thesis is to obtain a better understanding of how radiation damages tungsten and tungsten alloys by comparing material properties of these materials before and after radiation as well as determining effective methods to obtain these material properties. Existing literature was reviewed to compare the differences in material properties of virgin and irradiated tungsten. Additionally, numerical analyses were performed on tungsten and tungsten-rhenium to determine indentation modulus. Abaqus was used to run finite element simulations and complex mathematics to replicating a series of indentations about the material of interest was coded into Python. The input of both of these methods were the elastic constants of the material in question, either tungsten or tungsten-rhenium, and the output was the indentation modulus.

Key words: Nanoindentation, Tungsten, Python, Abaqus, Indentation Modulus

ACKNOWLEDGEMENTS

I would like to thank the Shackouls Honors College and Dr. Seth Oppenheimer for encouraging me to go beyond the minimum requirements for my degree. Thank you to Dr. Matthew Priddy and the Bagley College of Engineering for providing me the opportunity to participate in this research.

TABLE OF CONTENTS

LIST OF FIGURES

CHAPTER 1

INTRODUCTION

1.1 Motivation

While it is useful to have an understanding of the properties of an unaltered material, realistically, materials do not maintain these natural or virgin properties throughout their usage as they are exposed to conditions that may cause damage[1]. Examples of such damage range from general wear of a material to radiation exposure. Understanding the effect radiation has on a material's properties is significant for a variety of applications, including military use and nuclear energy plants. By studying irradiated materials and increasing the available data about properties of irradiated materials, the potential exists to decrease the impact radiation has on shortening the length of a material's useful life[2]. While different components of nuclear reactors require varying useful lives to be commercially viable, the common acceptable life for first wall components (which are typically composed of tungsten) range from two to five years[3].

The focus of the present study is to obtain a better understanding of how radiation damages tungsten and tungsten alloys by comparing material properties of these materials before and after radiation as well as determining effective methods to obtain these material properties. Because of limitations in resources, this research seeks to investigate existing literature to compare the material properties of virgin and irradiated tungsten and to perform numerical analyses on tungsten and tungsten-rhenium to determine indentation modulus. These analyses include performing a finite element simulation using Abaqus and using complex mathematics to replicate a series of indentations about the material of interest.

1.2 Understanding Nuclear Reactors

A variety of energy sources for electricity production exist, from the more common fossil fuels to solar and wind power. Of these different types, nuclear energy is one of the most controversial forms of energy that is currently used because of the fear that surrounds radioactive materials. In the United States, nuclear plants were first built and used in the late 1950s and had productive life expectations of thirty to fifty years. At the time, the need to decrease fossil fuel use and decrease the amount of air and land pollution allowed for the popularity and acceptance of such nuclear reactors. In some cases, nuclear reactors consume over a million times less fuel than coal-fired plants to produce the same amount of energy[7]. In 2017, about twenty percent of the electricity generated in the United States was nuclear. France currently relies on nuclear power for seventy-five percent of the nation's energy[8]. Figure 1 below shows a map of the locations of the 99 commercial nuclear reactors. However, the presence of nuclear reactors is declining within the United States for a number of reasons, including public perception and the improved feasibility of solar and wind energy[8,9]. The long half-lives of the products from the nuclear reactors require decades to centuries of secure storage[7].

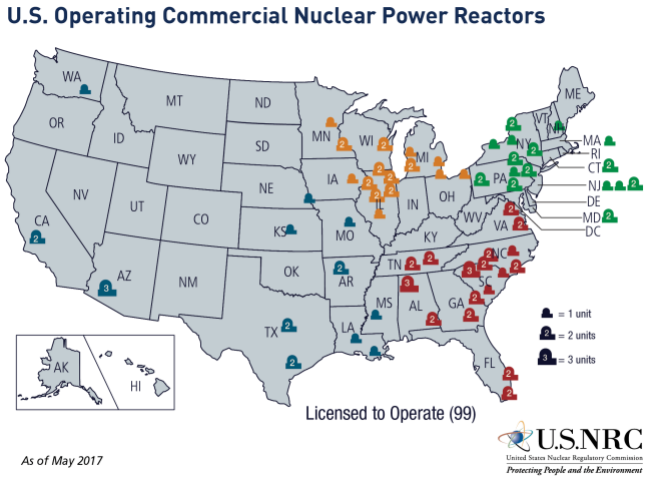

Figure 1. A map of the 99 commercial nuclear power reactors in the United States as of May 2017[10].

Nuclear reactors obtain energy in the form of heat from fission reactions that occur within the core of the reactor. Heat is created from the fission reactions in the nuclear reactor and transferred to water that is pumped past nuclear fuel rods[11]. The heated water turns into steam that generates work through a turbine.

1.3 Fission

Nuclear power plants are powered by the thermal energy created during nuclear fission. Figure 2 shows a diagram of neutron-beam fission radiation.

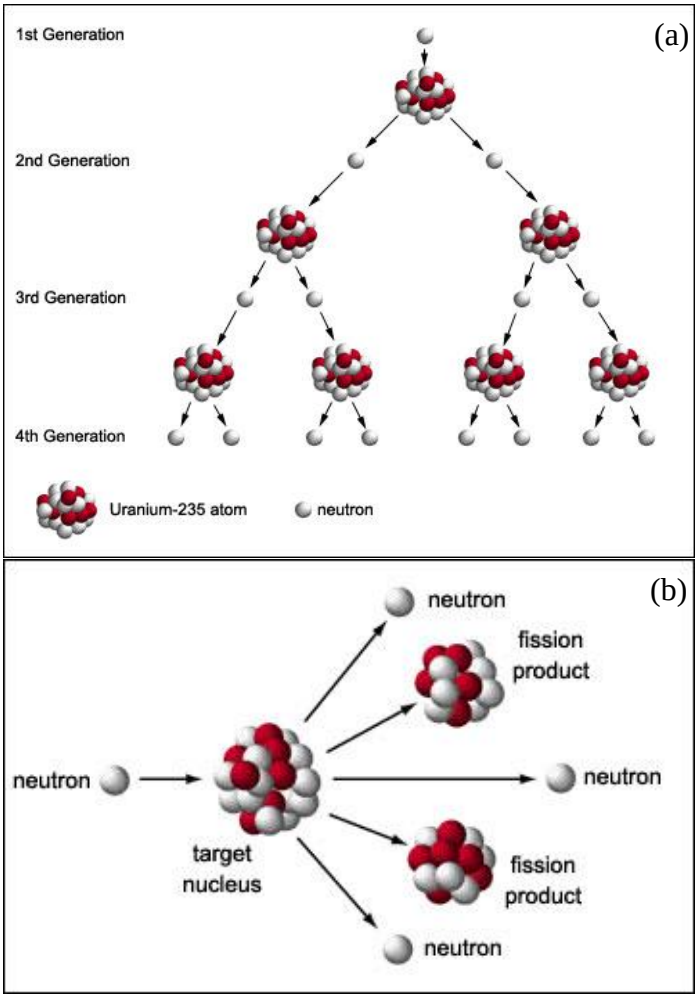

Figure 2. Nuclear fission (a) chain reaction and (b) single reaction[14].

During fission, a nucleus is hit with another particle, typically a neutron. As a result, the original nucleus is split into different product nuclei, which have new properties than the original nucleus. In addition to these product nuclei, neutrons are also released, which act to continue the fission process by hitting more nuclei and repeating the process. The product of the reactions differs based on the identity of the original nucleus. Uranium isotopes are commonly used as nuclear fuel, with uranium-235 being the best for fission chain reactions. However, only about 0.7% of uranium is uranium-235, so it is not a widely available resource[11,14].

Another consideration for fission chain reactions is the containment of the reactions, both through moderators and shielding materials. To slow down the fission chain reaction so that the temperature of the reactor may be controlled for safety purposes and to aid in the ability of harnessing all of the energy produced, moderators such as water or heavy water, water whose hydrogen atoms are replaced by deuterium (a hydrogen isotope), are placed within the uranium[11]. The moderator absorbs neutrons from the fission reactions to prevent them from striking uranium nuclei to continue the reaction. However, a balance must be obtained to ensure that enough neutrons are hitting uranium nuclei to continue the fission without allowing too many to hit uranium nuclei so that the reactions do not all happen too quickly to be able to effectively use the thermal energy produced. Shielding materials surround this fission reaction site to control which materials the neutrons hit, as well as to contain the area where irradiated materials exist. Because of the nature of their use, both moderators and shielding materials are hit with neutrons during the fission process. This causes a change in identity and properties for the nuclei of these two materials that are impacted.

Much of the fear surrounding nuclear energy is the association with nuclear weapons, which is out of the scope of this investigation, and the fear of radioactive leaks. Small leaks in nuclear reactors are inevitable because it is difficult to perfectly seal reactors, which allows radiated gas to escape. For a population of 300 million, it is estimated that these inevitable emissions cause 25 additional cancer deaths in the US per year[12]. However, it is also important to consider the consequences of pollution from other energy sources, such as air pollution from coal plants.

CHAPTER 2

PROBLEM BACKGROUND

2.1 Experimental Radiation

Materials in nuclear reactor environments would typically be exposed to neutron-radiation, however, this is unrealistic to recreate in a lab setting for experimentation. Neutron-radiation causes materials to become radioactive, and therefore, more difficult with which to work[4]. Acquiring the specific neutrons with the correct energy levels to simulate the setting is difficult, which is cost prohibitive[5]. While a few studies have suggested that with current technology, it is not possible to achieve levels of irradiation displacement per atom (dpa) considered realistic for a nuclear reactor setting in experimentation, this has not proved to be consistent with most of the literature[6].

Ion-beam radiation is one of the only methods currently available that does not cause hazardous activation of irradiated materials[6,15]. This form of radiation is also beneficial for research purposes because of the relatively low cost and quick time required to irradiate materials. Because ion-beam radiation employs low energy ions (over four times lower than neutron radiation)[16], the depth of material impacted by ion-beam radiation is significantly decreased[5,15,17]. As a result, the methods by which these irradiated materials are tested are limited by this small irradiated portion of the material to methods that are able to allow its isolated access and manipulation.

A significant issue noted when reviewing a number of studies performed on irradiated tungsten was the inconsistencies between different studies. While most studies stated a goal of better understanding the properties of irradiated tungsten, the magnitude varied of irradiation displacement per atom (dpa) from 0.01 to around 100 dpa[15,18]. The radiation type, speed, and dose

all significantly impact the change in material properties of the tungsten, making the results from these differing methods incomparable without additional data from a control study. In addition, the temperature at which the material was irradiated impacts the alteration of the material—notably, an increased temperature was observed to result in larger voids and a lack of dislocation loops[19,20].

Varying types of reactors impact the nature of the fission chain reaction. Fast-neutron reactors (FNR) do not use moderators to slow the neutrons in the fission process down, hence their name, while light water reactors do[11,21]. Studies comparing the results of a FNR (JOYO) and a mixed spectrum reactor (HFIR) observed differences in changes to material properties of the sample, with a decrease in material hardening and an increase in electrical resistivity of materials irradiation with the FNR[22,23]. In addition, the irradiation dose within a material is not always uniform. This uniformity is largely dependent on the type of ions employed in radiation, as heavier ions decrease homogeneity[24].

It is widely agreed that nanoindentation is one of the best methods to gather data about the material and mechanical properties of the isolated irradiated material, however the process of material preparation and implementation of indentation—including the indenter tip and size used—differs among studies and has been continually modified since the implementation of nanoindentation technology[5,16,24–26]. This continual change and modification occurs because of new understanding about the implementation of the nanoindentation method, namely the effect of plastic deformation on the sample and the relationship to indenter tips, that allows for the most repeatable measurements.

2.2 Spherical Nanoindentation

Although studies exist in which the properties of irradiated tungsten are investigated using spherical nanoindentation, they are limited and do not follow a standard procedure that makes them easily comparable. Because of this, published works whose focus was on materials other than tungsten, which have well documented properties were used to better understand nanoindentation processes as well as to validate results. Studies using spherical nanoindentation were performed on titanium because of the presence of the distinct α and β phases within the material and the microscale at which they can be distinguished[27]. These phases may be seen in Fig. 3.

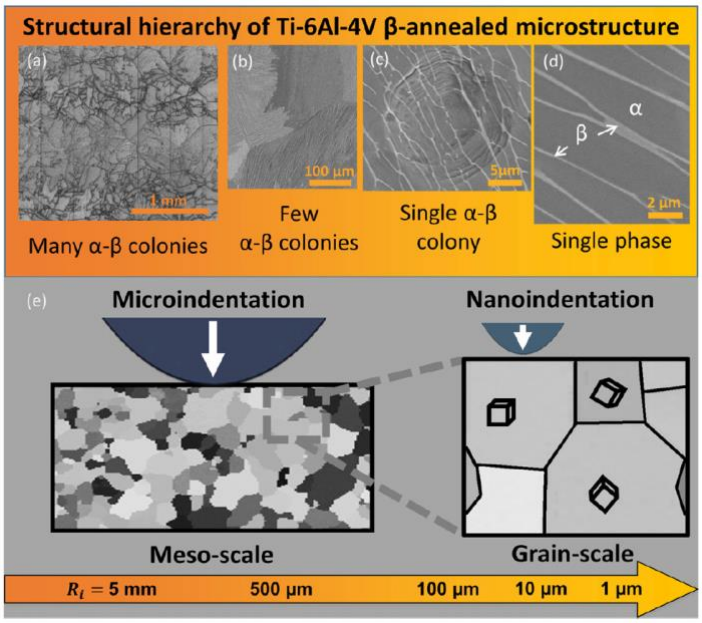

Figure 3. A comparison between micrometers and nanometers in distinguishing between α and β phases of titanium[27].

Prior to testing, a material's surface is polished to decrease roughness or deformation that impact the results of nanoindentation results. The comparison of (i) a mechanically polished with a colloidal silica suspension and hydrogen peroxide mixture polish and (ii) an electropolished

titanium sample showed the minimal effect of the polishing method because of similar indentions[27]. Electro polishing is a common preparation method for materials to be tested through spherical nanoindentation because it does not cause mechanical damage to the material[27]. Materials irradiated with ion-beam radiation are not able to be polished prior to nanoindentation because the polishing removes a significant amount of the irradiated material[18]. These materials should be polished prior to radiation exposure, should polishing be desired.

Many studies using nanoindentation employ Berkovich tips to find hardness of a material[4,6,18,25,28,29]. While this information is useful, load-displacement data collected with a Berkovich tip is difficult to gather and convert to meaningful graphs because of the plastic deformation that hinders the accuracy of results[1,18,30]. Recent studies have noted the significance of the use of spherical indenter tips to gather more relevant load-displacement data about a material's properties[4–6,18,25]. One such example is that spherical indenters allow for the interpretation of the load-displacement data into an indention stress-strain curve[18]. Spherical tips allow for deeper indentions and greater loads to be applied, aiding in the identification of the transition from elastic region to plastic region[18]. Studies comparing the results of spherical nanoindentation and Berkovich nanoindentation found agreement in the hardness and elastic modulus values calculated, but discrepancies in yield strengths, namely that yield strengths found with spherical indenters are around two times smaller[18,31,32]. It has been suggested that a synthesis of the two—using both Berkovich tips and spherical tips—in an experiment will result in a fuller set of data about a sample's material properties and information because the data acquired may be compared to ensure accuracy where a method is weak or lacking[5,33]. Because of these differing opinions on the relevance and usefulness of various indenter tips, inconsistencies exist among studies in the nanoindentation methods employed to gather data about material properties.

Studies on virgin materials that used a variety of indenter sizes found that no significant relationship existed between the size of the indenter used and both the yield strength and indentation modulus calculated[27]. It is significant to note, however, that smaller indenter tips are more favorable because they allow the use of continuous stiffness measurement to avoid full or partial unloading when determining contact radius[27]. For irradiated materials, varying indenter sizes, including relatively large indenters, is critical to understanding a variety of material and structural properties about the nature of the radiation effect. Figure 4 shows the impact of varying indenter sizes on Ti-64 by emphasizing the area of impact, a, for each radius size, R_i.

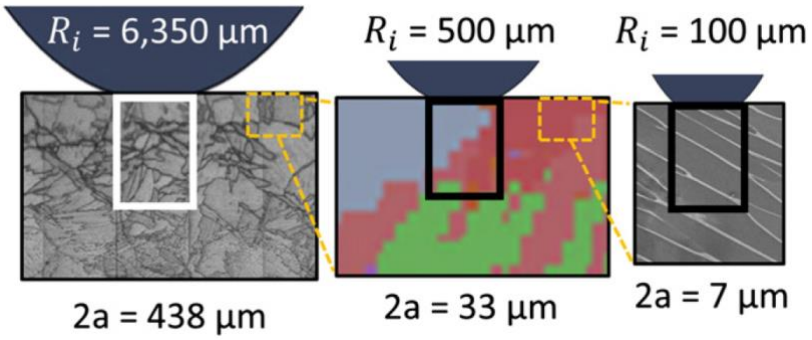

Figure 4. Indentation zone and structural length scales of different spherical indenter radii for β-annealed Ti-64[27].

Beyond these changes to the physical process of nanoindentation, recent studies have also found benefits from alterations to the type of data gathered during testing. In addition to indentation modulus, the hardness of a material is a commonly found property in nanoindentation studies because it is relatively easy to obtain hardness data for a range of materials[34]. However, because of the way in which hardness is found—standardized test parameters employed to combat an arbitrary strain and the large presence of plastic deformation—and the relative usefulness of hardness as a calculated variable, some studies instead elect to consider indentation yield

strength[30]. Indentation yield strength requires no standardized test parameters and is found before any plastic deformation occurs, therefore making it a more reliable and relevant variable to use[30]. Spherical nanoindentation allows the collection of data concerning the elastic modulus, both loading and unloading and indentation yield strength for a material in its pure form and after damage caused by radiation[1].

As a whole, nanoindentation is limited because of the stress caused around the indention on the material, which causes the results to be incomparable to the material in bulk form[4]. Nanoindentation in general must be very precise to ensure correct depth—deep enough to gather relevant information but not too deep to be influenced by virgin material[5]. In addition, the change in indenter sizes necessary to study the differing layers of virgin and irradiated materials impacts the hardness measured[24].

As briefly mentioned, these preliminary considerations for the most reliable and accurate implementation of spherical nanoindentation methods must be altered when considering irradiated materials. As shown in Fig. 5a, Helium ion radiation has been shown to impact a material by creating three new layers at the surface of the material—two transition layers sandwich a layer of high radiation impact[1]. To determine the depth of the radiation impact as well as the transitional layers in the material, a series of indenters of differing radii (1, 10, and 100 micrometer) were used[1]. The impact of varying indenter sizes is also shown in Fig. 4, which calls attention to indentation zone and structural length scales of three different indenter radii.

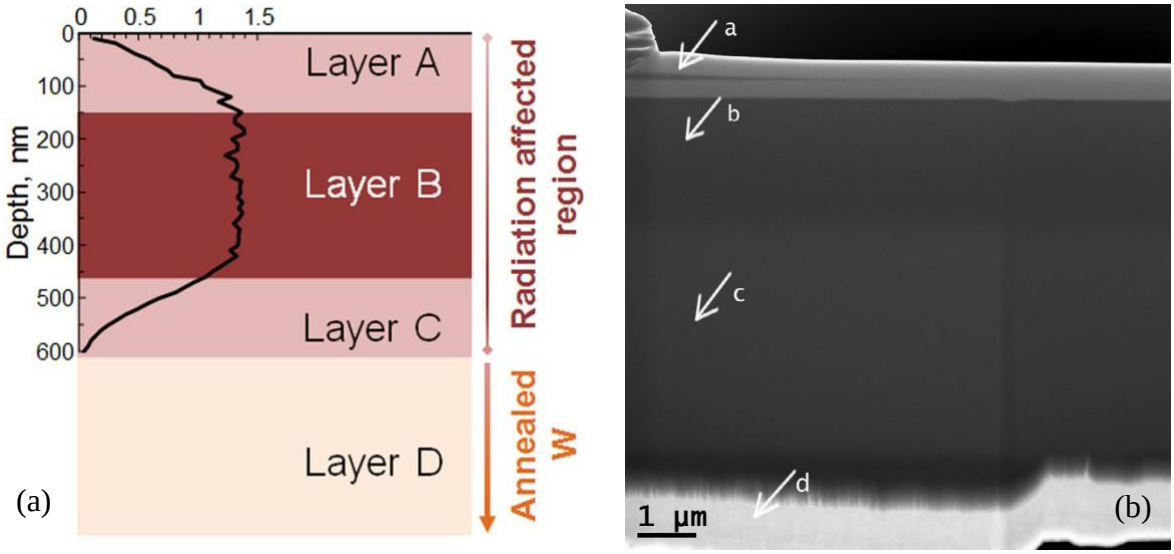

Figure 5. Layers in Tungsten caused by radiation damage. (a) He radiation with transitional layers A and C, heavily radiation damaged layer B, and virgin layer D[1]. (b) Self-ion irradiation[15].

Smaller indenters (of radius ~1 micrometer) penetrate the material only to the top layer, providing information about its indentation yield strength[1]. As larger indenters are used, the penetration depth of the indenter increases, providing similar data about other layers. In addition, the comparison of this information (yield strength and hardness) between the varying indenter sizes allows for the depth of each layer to be calculated[1].

Not every type of radiation causes this same formation within a material. Fig. 5b shows layers formed in tungsten irradiated by tungsten ions. Rather than transitional layers above and below the heavily damaged radiation layer (b), there are two amorphous layers of tungsten (a) above the radiation and a virgin, undamaged layer below (c). Below the undamaged material there is an additional layer of re-deposited material. Both layers (a) and (d) were caused by the focused ion beam extraction method used in the study[15]. It is also significant to note that the relative thicknesses of these two radiation types are on different orders of magnitudes. The irradiated layer of tungsten shown in Fig. 5a is 600 nanometers thick, compared to the almost 2 micrometer (2000

nanometer) thick irradiated layer shown in Fig. 5b. Given the difference in scale, Fig. 5b could just be including the transitional layers distinguished in Fig. 5a as part of the heavily radiation damaged layer. It should be noted that this is another form of inconsistency among studies of this nature.

At shallow indentation depths (such as indentions in layer A of Fig. 5a), the assumptions made about contact depth must be changed. The amount of the indenter that is in contact with the material is much smaller at smaller indentation depths. Understanding the correct depth to use in hardness calculations is critical to ensuring accurate hardness values. Figure 6 shows three different depths associated with an indentation.

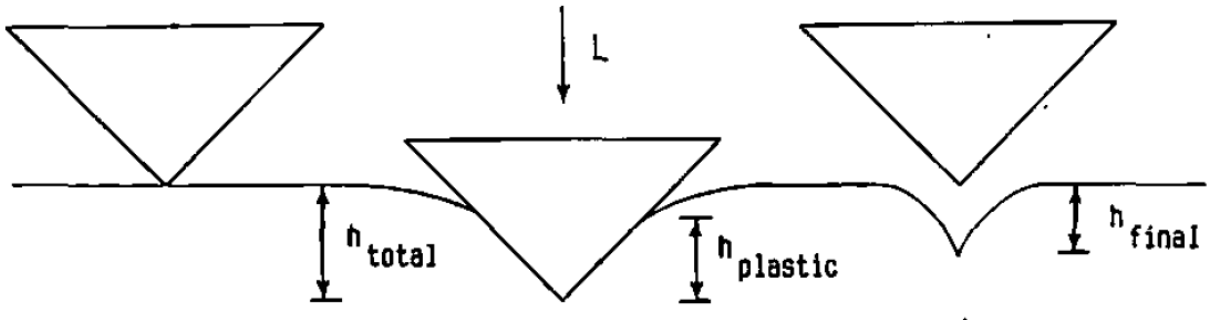

Figure 6. Defining total, plastic, and final indentation depths[35].

Based on the definitions in Fig. 6, using the final depth instead of the plastic depth would significantly increase the hardness measured to an inaccurate overestimate.

In studies of irradiated materials, orientation of the grains have been found to have significant impact on the effect of the radiation and, therefore, the differences in values of material properties, including indentation yield strengths[1]. Accuracy of data gathered through the methods discussed may be increased by performing multiple indentions on a material under constant conditions and/or excluding data from samples whose indentation site was near grain boundaries[1].

2.3 Tungsten and its Alloys

As radiation impacts a material, it causes defects that change both its material and mechanical properties. The type and extent of these defects is largely dependent on the microstructure of the material. FCC and BCC materials experience a difference in defects, namely stacking fault tetrahedral (SFT) and interstitial loops, respectively[2].

When considering shielding materials to use in settings such as nuclear reactors, it is important to consider materials that are able to withstand the temperatures and conditions of a radiation environment before and after the absorption of radiation[36]. Tungsten is commonly used because of its positive performance when exposed to high temperatures and high particle fluxes[4,15,36,37]. The melting point of tungsten is over 3000 degrees Celsius[6]. In addition, tungsten has a large resistance to erosion and sputtering[3,22,38]. Implications of irradiated tungsten have significant impact on nuclear power plants. In the setting of nuclear reactors, tungsten commonly experiences both self-ion irradiation and helium ion irradiation[3]. Studies that compared hardness and yield stress for virgin tungsten, self-ion irradiated tungsten, and W and He ion irradiated tungsten showed that that while yield stress remained similar for all three, hardness values differed more significantly (increased with radiation exposure)[25]. Because, in virgin materials, it is common to observe a correlation between hardness and yield strength, the lack of this observation for the irradiated tungsten is notable[25].

The dislocation loops caused by radiation damage had no notable impact on the yield strength of the different samples, however, the voids and dislocation loops increased the measured hardness of the materials[25]. Materials exposed to neutron radiation experience transmutation, a process through which the material absorbs a neutron and consequently emit energy. During transmutation, new are formed because of the introduction of the neutron. The voids caused by the

irradiation of the tungsten are filled during the radiation and transmutation process by ions, such as rhenium and osmium, increasing the hardness and impacting other material properties of the sample[22,25]. Figure 7 shows the variation of the precipitates within the voids with the depth of the irradiated sample, as well as the non-uniform nature of radiation and the impact of indentation on the sample.

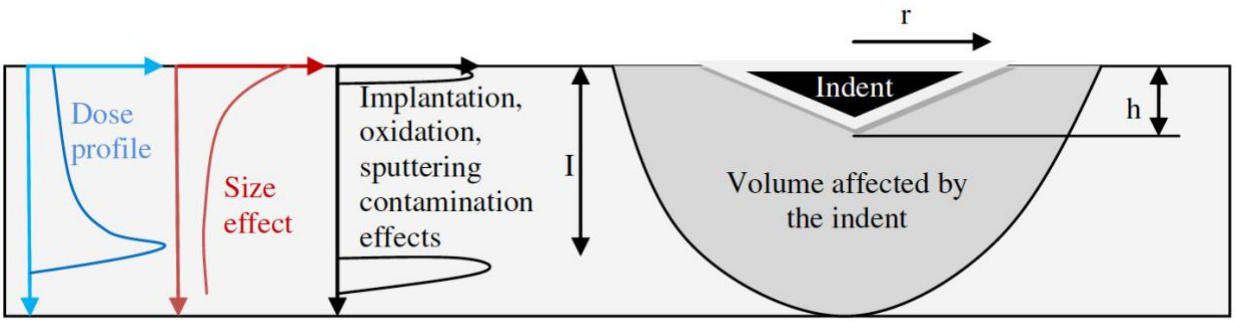

Figure 7. Radiation and indentation effects of irradiated surfaces at a nanoscale. Dose profile, indentation size effect, contamination effects, and volume impacted by indenters are shown[24].

Irradiated tungsten experiences an increase in brittleness caused by the radiation damage[3,39]. To increase ductility, before and after radiation exposure, tungsten may be alloyed with one of several different elements, including rhenium. Rhenium is often combined with tungsten because of the desirable material properties, including ductility, hardness, and mechanical resistance[3,37]. However, the presence of other elements, such as rhenium, in virgin tungsten impacts the way in which it reacts to radiation damage[6].

Pure tungsten and tungsten-rhenium alloys differ after radiation exposure because of the nature of the void formations within the two materials[37,39]. The irradiated tungsten-rhenium alloy was not found to have structural damage dominated by the voids, suggesting the addition of the rhenium helps to reduce or prevent these voids[19,20,39]. Tungsten-rhenium alloys have also been

observed to have decreased hardening and fewer dislocations than pure tungsten when exposed to radiation[19,20]. Additionally, these irradiated alloys experience fewer precipitates, at smaller densities[19,20]. While rhenium in tungsten has a solubility limit of twenty-six percent, varying the weight of rhenium in the W-Re alloys was not found to have an impact on irradiation effect[19,20].

One reason for the differences between irradiated pure tungsten and tungsten alloys is that the products of transmutation differ based on the starting elements present. Figure 8 shows a comparison of the transmutation products of tungsten and a tungsten-vanadium alloy. The additional presence of vanadium in the tungsten alloy causes the presence of elements, such as titanium and chromium, not seen in the pure tungsten sample after transmutation.

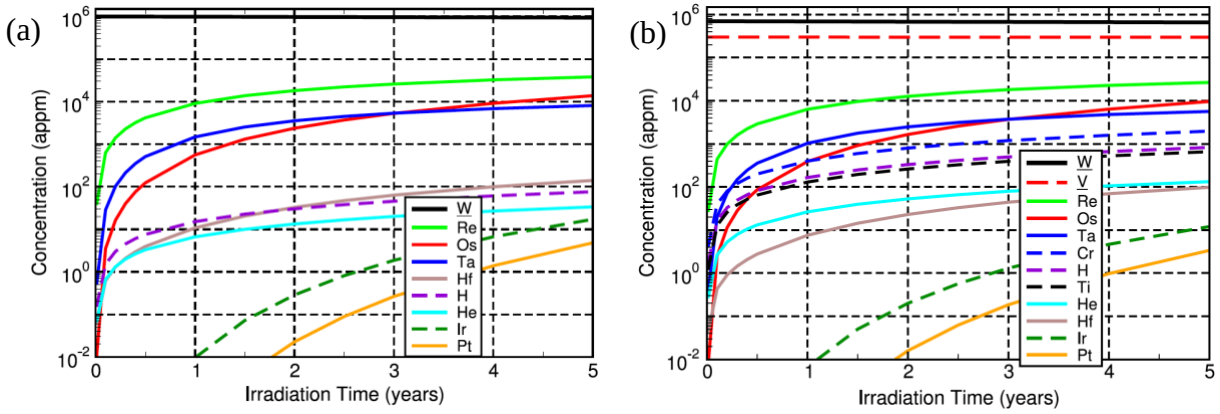

Figure 8. Concentration of elements present in (a) W and (b) W-30% V after transmutation under conditions of a fusion power plant[3].

The products of the transmutation differ based on the composition of the virgin material[3,39]. A comparison of the transmutation products of pure tungsten and tungsten - 30% rhenium alloy reveals that the alloy has an additional product of osmium[3]. Osmium is not a desirable product because of the negative effect it has on both mechanical and structural properties[3]. Studies also

noted that while tungsten-rhenium alloy did not cause a significant change in the amount of the transmutation products compared to those of pure tungsten, other alloys caused an increased transmutation production of helium and hydrogen gases[3].

2.4 Summary of Literature Review

After reviewing the literature, it is evident that there is not a well-developed process for performing research in this field. Table 1 displays the differences between seven different studies on irradiated tungsten.

Table 1. Differences in Radiation Conditions across Literature.

Study Author	Reactor Type	dpa	Radiation Type	Temperature
Armstrong	DEMO	1.0	Self-ion, Helium ion	800℃
Barabash	Mixed spectrum	0.3 – 0.5	Neutron	200 - 1000℃
Ciupinski	Tandem Accelerator	0.01, 0.1, 0.89	Self-ion	27℃
Fukuda	HFIR	1.0	Neutron	500, 800℃
Hasegawa	JOYO (fast), JMTR, HFIR (mixed spectrum)	0.15 – 1.0	Neutron	500 – 600℃
He, Tang	JMTR (mixed spectrum)	0.15	Neutron	600, 800, 1000℃
Hosemann	Danphysik ion implanter	1.0	Proton	50℃

From the table, it is clear that a variety of conditions under which a material is irradiation for research exist. The type of reactor (fast, slow, or mixed spectrum), the strength and type of radiation, as well as the temperature at which the material is irradiated all impact the way in which a material is damaged by radiation.

CHAPTER 3

RESEARCH METHODS

3.1 Research Focus

The purpose of this research is to investigate the indentation modulus of both tungsten and tungsten-rhenium alloys. Both analytical methods and finite element simulations are used to calculate the indentation modulus of both materials using inputs of the material's elastic constants. The results of both methods may be compared as well as used to ensure accurate results. As discussed with the different indentation tips and methods, a synthesis of solutions proves to be helpful when the strengths of a particular method overlap the limitations of another.

Because the focus of this work involves understanding the impact of radiation on the material and mechanical properties of materials that are commonly exposed to radiation, the initial goal was to use the published elastic constants of tungsten and various tungsten-rhenium alloys as well as their irradiated counterparts. However, the elastic constants of irradiated tungsten and irradiated tungsten-rhenium are not well documented and were not able to be included.

3.2 Finite Element Analysis

Finite element analysis is a common engineering tool used to model different physical phenomena. For the purposes of this investigation, considering finite element models (FEM) to replicate or replace potential experimental studies using nanoindentation to examine the properties of irradiated materials may allow better results because of the previously discussed limitations of nanoindentation. Many studies comparing experimental results of nanoindentation technology with calibrated results of finite element models found the data from both methods to have negligible differences[26,34,40,41]. Figure 9, shown below, provides one such comparison of load-

displacement results of two different materials, nickel and silicon, from experimental methods and finite element analysis.

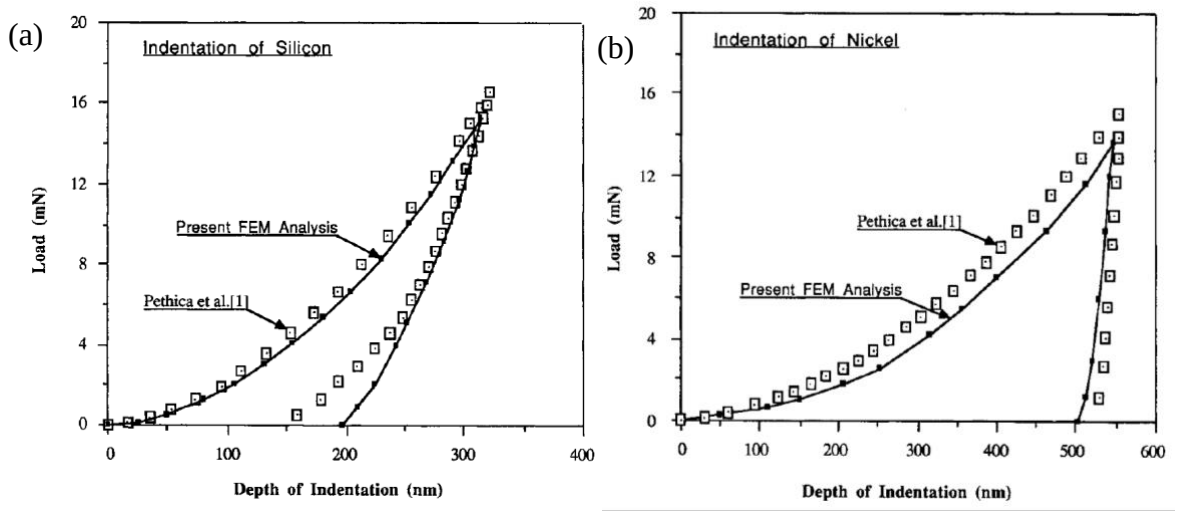

Figure 9. Comparing experimental and FEM load-displacement graphs of (a) silicon and (b) nickel[34].

To implement such a model several different factors must be considered, including (i) the size and (ii) shape of the indenter, (iii) the contact between the indenter and the sample, and (iv) the mesh size of the sample. Many of the current studies using FEM assume indenters that are perfectly rigid[28,34,42]. In addition to this assumption, it is necessary to decide which indenter tip to use in the simulation. Studies that compared experimental data with FEM did so using a Berkovich tip, and as a result began simulations assuming a sharp indenter tip[26,28,43,44]. However, several of these studies also made a note of this perfect sharpness as a limitation and also ran simulations using a conical tip that had the same projected area as the Berkovich indenter[26,43,44]. Figure 10 below shows a comparison between slightly rounding the tip of the indenter and using a perfectly sharp indenter. As indicated in the figure, the FEM with the rounded indenter reflects experimental

results, while the sharp indenter shows significant difference. Although theoretically Berkovich indenter tips are sharp, realistically they have a rounded tip with a radius of curvature around 150-200 nm because of sources of errors, such as manufacturing restrictions[26,45].

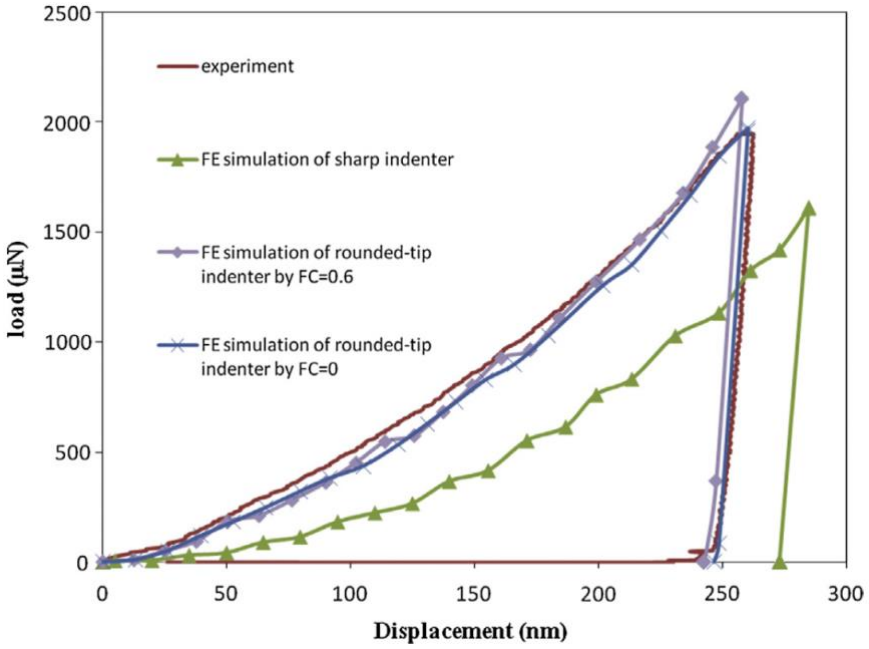

Figure 10. A comparison of experimental and varying tips of finite element analysis load-displacement results of aluminum 1100[26].

Tip sharpness also has a large impact on stress and twinning in the material. Blunt tips cause larger stress near the point of contact, while sharper tips on the basal plane increase the likelihood of twinning for materials that have a propensity to twin[43].

Another component to consider when running simulations is the contact between the indenter and the material used in the sample. Studies performed on nickel, silicon, and aluminum showed no significant difference when assuming a variety of friction coefficients, therefore the contact between the two was assumed to be frictionless sliding interface[28,34,42]. Frictionless contact was found to be a valid assumption for large angle indenters as well[42].

Mesh size must be determined for the analysis to ensure fine enough mesh to gather accurate results without a mesh that is so small it causes simulations to run for extended lengths of time. Most studies noted that the finest mesh used was near the indenter contact surface and mesh size increased as the distance from the indention increased[34,42,45]. When choosing a mesh size, it is critical to ensure that no significant changes in variables being studied, such as a load-displacement curve, occur when mesh size is decreased. The amount of brick shaped elements used to model the material ranged widely from 461 to 23,000 eight-node linear brick elements[34,45]. In addition, discrepancies were noted between studies who opted for three-dimensional meshes[44,46] as opposed to using a two-dimensional model and assuming the indenter and the sample are bodies of revolution[34]. Once the parameters of the simulation have been established, the indention is modeled by giving the indenter a downward and upward displacement to replicate applying a force with the indenter on surface of the material.

For this research, Abaqus (a finite element software package) was used to perform a finite element simulation of spherical nanoindentation of a small block of material. Figure 11 shows the spherical indenter on top of the rectangular specimen, both (b) in Abaqus and (a) rendered to show a clearer image of the process.

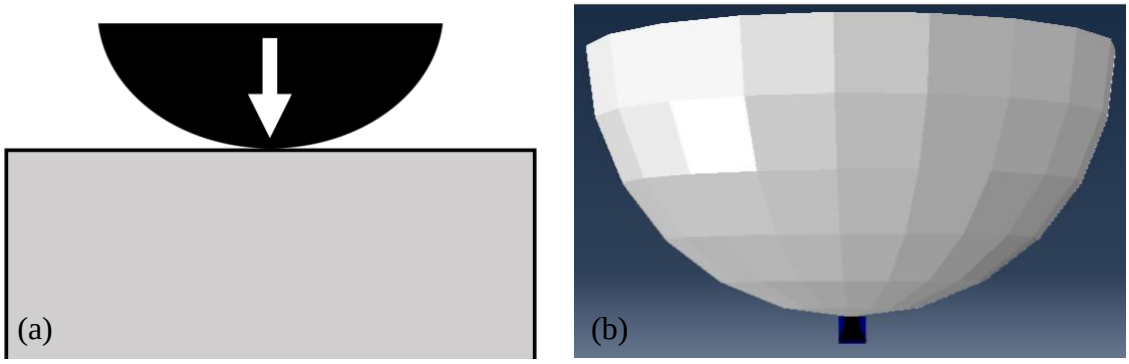

Figure 11. (a) Two-dimensional profile of spherical nanoindentation. (b) Spherical indenter on top of the block of material in Abaqus.

To perform the simulations in Abaqus, a mesh was created for the block of material of interest. The mesh in these simulations is shown in Fig. 12 and includes both finite and infinite elements.

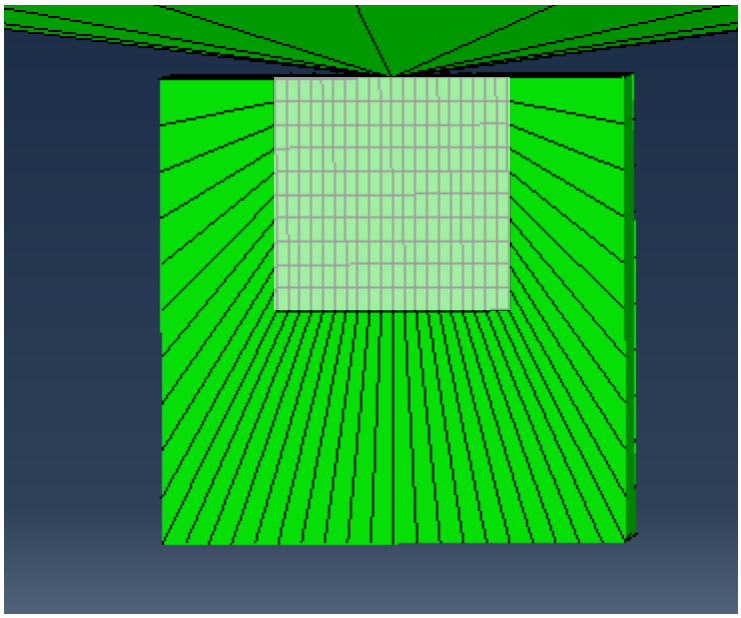

Figure 12. Mesh used to examine the material during simulations.

The finite elements are shown by the pale green blocks in Fig. 12 while the infinite elements are the outer, lime green colored parts of the cube. The use of infinite elements within the mesh helps to minimize the impact of the boundary conditions on the indentation modulus. Because the indenter is spherical, the contact between the specimen and the indenter was modeled to be frictionless.

This program was created so that the nanoindentation process remained the same, while different material properties were assigned to the block to simulate tungsten and alloys of tungsten. The elastic constants of these materials were obtained from published works and used to code the simulation in Abaqus. For each simulation, the indenter was programmed to have a set displacement of 1.0 nm to load and 0.1 nm to unload the indenter on the block of material. Data

from this displacement and the corresponding force experienced by the block of material were collected during each simulation for the initial unloaded step, the loaded step and for the final unloaded step post-test. The data collected during the simulation was then exported to Microsoft Excel and calculations were performed to determine the indentation modulus of the material.

Equation 1 was used to convert the calculated force (F_{calc}) by raising it to the power of two-thirds.

$$F' = (F_{calc})^{2/3} \tag{1}$$

This modified force, F', was used with the corresponding displacements (δ) to calculate the slope (m) as shown in Eqn. 2.

$$m = \frac{\delta_2 - \delta_1}{F'_2 - F'_1} \tag{2}$$

Finally, Eqn. 3 was used to calculate the indentation modulus (E) using the calculated slope and the indenter radius.

$$E = \left(m^{-\frac{3}{2}}\right)\left(\frac{3/4}{\sqrt{r}}\right) \tag{3}$$

The radius (r) of the indenter used in the simulations was 13.5 micrometers.

3.3 Analytical Analysis using Python

A second analytical solution was considered to collect data about the indentation modulus of various materials. A Python script was developed based on the work of Franzoso (2008) that simulates spherical nanoindentation at varying angles about an anisotropic material. The indentation modulus for an anisotropic material is dependent on the material's elastic constants and the direction of indentation. By obtaining the published elastic constants of an anisotropic material, nanoindentations may be performed at a variety of angles to understand the indentation

modulus at all angles of the material. This process may be simplified by performing a mathematical analysis using a series of equations, whose input is the material in question's elastic constants. One specific method is an analytical solution which takes a material's elastic constants and performs iterations to determine the local indentation modulus while rotating about the material. The mathematics behind this solution are detailed below and has been coded in Python and published for public use.

To understand this mathematical analysis, the basic principles behind the indentation modulus must be understood. Anisotropic materials, by nature, require more elastic stiffness constants to be defined than isotropic materials. Rather than individually performing nanoindentations at different angles on the material, mathematics may be performed to calculate the indentation moduli. These values may then be graphed to provide a visual of the changes in indentation modulus throughout the material. The elastic stiffness tensor, $\mathbb{S}$, is the input and provides information about orientation.

During this process, several reference coordinates are defined to perform the rotation about the material. Figure 13 shows these reference coordinates, where the coordinates (e_1, e_2, e_3) indicate the coordinate system of the material, (e_1`, $e_2$`, e_3`) indicate the initial coordinate system, and (a_1, a_2, a_3) indicate the corrected coordinate system.

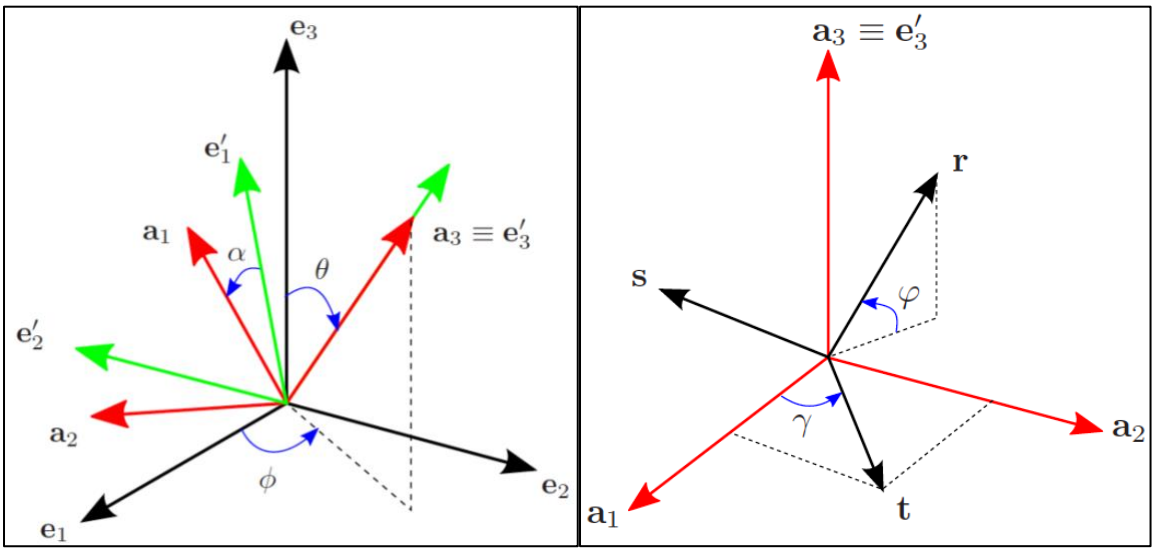

Figure 13. Reference coordinate systems for mathematical analysis of anisotropic materials[47].

A positive-definite tensor, $B(t, \mathbb{S})$, is defined using the (r, s, t) coordinate system (also shown in Fig. 13) whose inputs are the elastic stiffness tensor and t. $B(t, \mathbb{S})$ is defined so that it considered the elastic properties of the material.

$$B\ (t, \mathbb{S}) = -\frac{1}{2\pi}\int_0^{2\pi}[(rs)(ss)^{-1}(sr) - (rr)]d\varphi \tag{4}$$

The ellipse ratio, ${}^{a_1}/_{a_2}$, is given by Eqn. 5 and is solved through iterations, where Eqn. 5 is assumed to be equal to one initially and a new value for ${}^{a_1}/_{a_2}$ is obtained and the process is repeated setting Eqn. 5 equal to this new calculated value.

$$\frac{a_1}{a_2} = \left(\frac{\pi}{2} \left[1 - 2 \frac{\int_{-\frac{\pi}{2}}^{\frac{\pi}{2}} \frac{(1 - |\sin\gamma'|) \cdot (B^{-1}(\gamma', \mathbb{S}) : [a_3 \otimes a_3])}{\sqrt{\left({}^{a_1}/_{a_2}\right) \cos^2\gamma' + \left({}^{a_2}/_{a_1}\right) \sin^2\gamma'}} d\gamma'}{\int_0^{2\pi} \frac{B^{-1}(\gamma, \mathbb{S}) : [a_3 \otimes a_3]}{\sqrt{\left({}^{a_1}/_{a_2}\right) \cos^2\gamma + \left({}^{a_2}/_{a_1}\right) \sin^2\gamma}} d\gamma} \right] \right)^2 \quad (5)$$

Ultimately, the indentation modulus, E, of the material is given by Eqn. 6 and is a function of the elastic stiffness tensor, $\mathbb{S}$, and the direction of indentation, a_3 [47].

$$E(\mathbb{S}, a_3) = \frac{4\pi}{\int_0^{2\pi} \frac{B^{-1}(\gamma, \mathbb{S}) : [a_3 \otimes a_3]}{\sqrt{\left({}^{a_1}/_{a_2}\right) \cos^2\gamma + \left({}^{a_2}/_{a_1}\right) \sin^2\gamma}} d\gamma} \quad (6)$$

The initial direction of indentation is assumed to be zero. After one value for the indentation modulus is calculated, the corrected reference coordinates become the new initial reference coordinates (in other words, the reference coordinates are rotated by α). This process is repeated to find a new value for $B(t, \mathbb{S})$, the ellipse ratio, and indentation modulus.

The code outputs each iteration so that the range of indentation moduli may be obtained and so that a three-dimensional graph may be plotted using the varying indentation moduli for the material. Along with the indentation moduli, the angle of indentation, the ellipse ratio, and angle of rotation (α) are all given for each iteration performed. As with the Abaqus simulations, the elastic constants for various materials (tungsten and tungsten alloys) were obtained from published works and used as inputs for the Python code. The code was run for each material and the output data were exported to be analyzed with Microsoft Excel.

CHAPTER 4

CONCLUSION

4.1 Confirmation of Methods

To ensure that the finite element simulations and analytical solutions were functioning correctly, these were both run with a well-documented material. Both the elastic constants and the indentation modulus of titanium are known values, so titanium was used for this purpose. The elastic constants of titanium used are listed in Table 2.

Table 2. Elastic Constants of Titanium.

Material	**Type**	**Elastic Constants (GPa)**					
		C_{11}	**C_{12}**	**C_{13}**	**C_{33}**	**C_{44}**	**C_{66}**
Ti-64	Tetragonal	162.2	91.8	68.8	180.5	46.7	35.2

These constants were input into Abaqus and into the Python code and the results of these simulations are compared with the accepted indentation modulus in Table 3.

Table 3. Indentation Modulus of Tungsten.

Material	**Type**	**Indentation Modulus (GPa)**		
		Analytical	**FEA**	**Accepted**
Ti-64	Cubic	121.1 – 142.6	122	120 – 145

From Table 3, it is evident that both the analytical solution and the finite element analysis of the indentation modulus are accurate models.

4.2 Visualization of Results

The elastic constants of tungsten and different tungsten-rhenium alloys gathered from different published works are displayed in Table 4. These values were used for both the simulations and the analytical solutions.

Table 4. Elastic Constants of Tungsten and its Alloys.

Material	**Type**	**Elastic Constants (GPa)**					
		C_{11}	**C_{12}**	**C_{13}**	**C_{33}**	**C_{44}**	**C_{66}**
W[48,49]	Cubic	522.4	204.4	--	--	160.0	--
W[50]	Tetragonal	466.0	259.0	180.0	545.0	93.0	95.0
$W_{0.75}Re_{0.25}$[37]	Cubic	550.0	217.0	--	--	156.0	--
$W_{0.75}Re_{0.25}$[37]	Tetragonal	540.0	235.0	212.0	552.0	89.0	128.0
$W_{0.50}Re_{0.50}$[51]	Cubic	427.9	278.9	--	--	222.0	--
$W_{0.25}Re_{0.75}$[51]	Cubic	485.9	273.7	--	--	299.0	--

Figure 14 displays snippets of the script from both the (a) Abaqus simulations and (b) the analytical solution. The elastic tensor values in both codes are of tungsten.

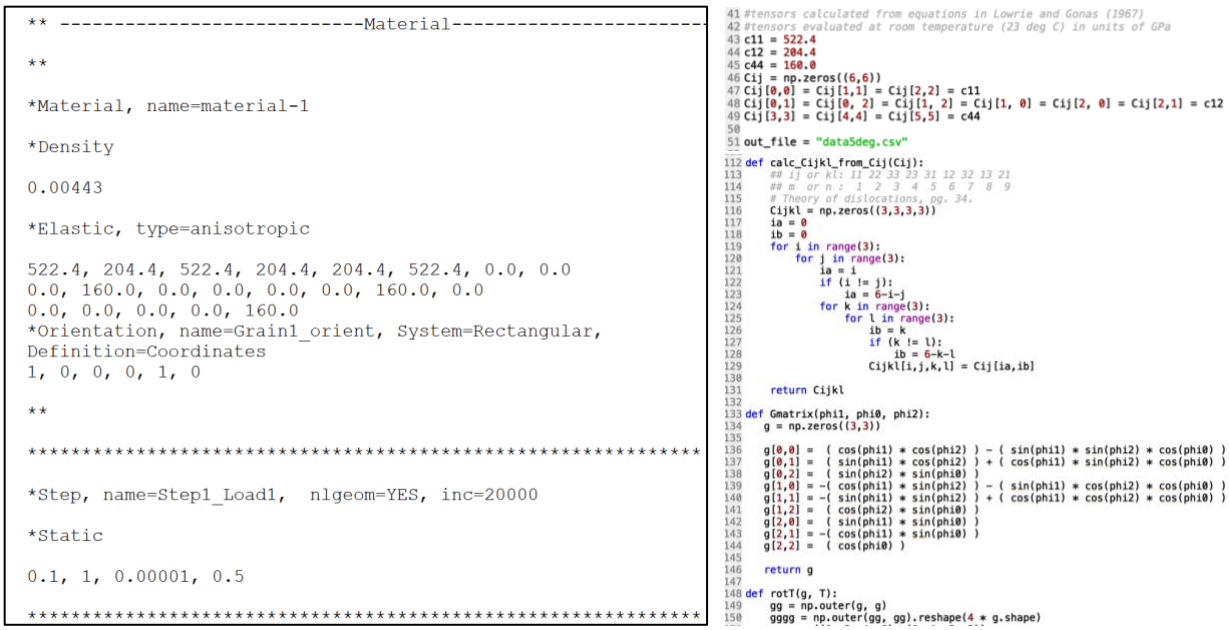

```
** ----------------------------Material-----------------------
**

*Material, name=material-1

*Density

0.00443

*Elastic, type=anisotropic

522.4, 204.4, 522.4, 204.4, 204.4, 522.4, 0.0, 0.0
0.0, 160.0, 0.0, 0.0, 0.0, 0.0, 160.0, 0.0
0.0, 0.0, 0.0, 0.0, 160.0
*Orientation, name=Grain1_orient, System=Rectangular,
Definition=Coordinates
1, 0, 0, 0, 1, 0

**

**********************************************************************

*Step, name=Step1_Load1,  nlgeom=YES, inc=20000

*Static

0.1, 1, 0.00001, 0.5

**********************************************************************
```

```python
#tensors calculated from equations in Lowrie and Gonas (1967)
#tensors evaluated at room temperature (23 deg C) in units of GPa
c11 = 522.4
c12 = 204.4
c44 = 160.0
Cij = np.zeros((6,6))
Cij[0,0] = Cij[1,1] = Cij[2,2] = c11
Cij[0,1] = Cij[0, 2] = Cij[1, 2] = Cij[1, 0] = Cij[2, 0] = Cij[2,1] = c12
Cij[3,3] = Cij[4,4] = Cij[5,5] = c44

out_file = "data5deg.csv"

def calc_Cijkl_from_Cij(Cij):
    ## ij or kl: 11 22 33 23 31 12 32 13 21
    ## m  or n :  1  2  3  4  5  6  7  8  9
    # Theory of dislocations, pg. 34.
    Cijkl = np.zeros((3,3,3,3))
    ia = 0
    ib = 0
    for i in range(3):
        for j in range(3):
            ia = i
            if (i != j):
                ia = 6-i-j
            for k in range(3):
                for l in range(3):
                    ib = k
                    if (k != l):
                        ib = 6-k-l
                    Cijkl[i,j,k,l] = Cij[ia,ib]

    return Cijkl

def Gmatrix(phi1, phi0, phi2):
    g = np.zeros((3,3))

    g[0,0] =  ( cos(phi1) * cos(phi2) ) - ( sin(phi1) * sin(phi2) * cos(phi0) )
    g[0,1] =  ( sin(phi1) * cos(phi2) ) + ( cos(phi1) * sin(phi2) * cos(phi0) )
    g[0,2] =  ( sin(phi2) * sin(phi0) )
    g[1,0] = -( cos(phi1) * sin(phi2) ) - ( sin(phi1) * cos(phi2) * cos(phi0) )
    g[1,1] = -( sin(phi1) * sin(phi2) ) + ( cos(phi1) * cos(phi2) * cos(phi0) )
    g[1,2] =  ( cos(phi2) * sin(phi0) )
    g[2,0] =  ( sin(phi1) * sin(phi0) )
    g[2,1] = -( cos(phi1) * sin(phi0) )
    g[2,2] =  ( cos(phi0) )

    return g

def rotT(g, T):
    gg = np.outer(g, g)
    gggg = np.outer(gg, gg).reshape(4 * g.shape)
```

Figure 14. Snippets of (a) Abaqus script and (b) Python script.

The finite element simulation produces both numerical data and a visualization of the material of interest's mesh throughout the simulation. Figure 15 shows images of the mesh of the tungsten (corresponding to the script in Fig. 14) during each of the three major stages of simulation: (a) prior to the test, (b) when entire load has been placed on the tungsten by the indenter, and (c) after the tungsten has been unloaded.

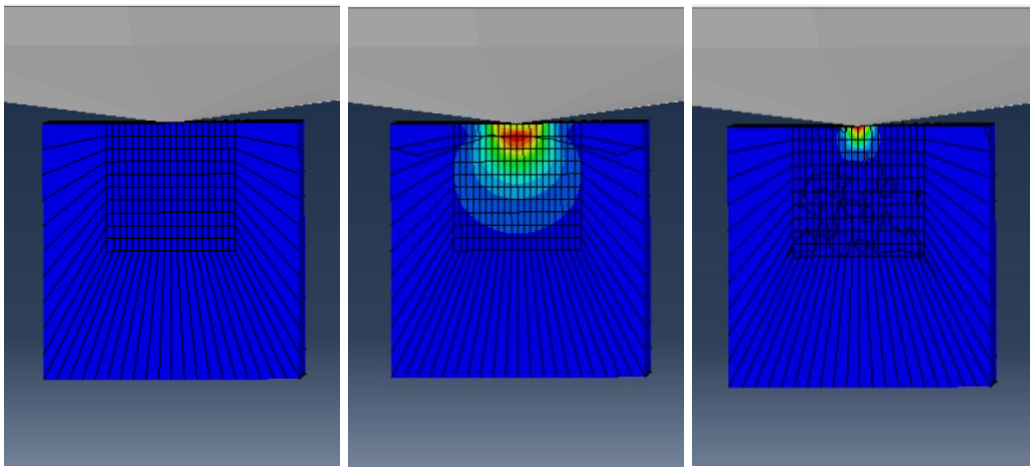

Figure 15. Visualization of a tungsten mesh (a) before testing, (b) loaded, and (c) after it has been unloaded.

The numerical results from the finite element simulations and the analytical solutions are listed in Table 5 below. Because the output of the Python code is multiple indentation moduli at a variety of angles, the average of these values was used for this table.

Table 5. Indentation Moduli from FE Simulations and Analytical Solutions.

Material	**Type**	**Indentation Modulus (GPa)**		
		Analytical Average	**Analytical Range**	**FEA**
W[48,49]	Cubic	443.57	443.45 – 443.71	380.68
W[50]	Tetragonal	339.23	320.99 – 372.51	389.03
$W_{0.75}Re_{0.25}$[37]	Cubic	451.76	450.41 – 452.97	359.72
$W_{0.75}Re_{0.25}$[37]	Tetragonal	365.34	355.26 – 382.06	359.72
$W_{0.50}Re_{0.50}$[51]	Cubic	401.62	384.10 – 423.18	330.99
$W_{0.25}Re_{0.75}$[51]	Cubic	514.08	490.33 – 543.33	422.28

From the literature, the maximum indentation modulus for tungsten is around 380 GPa[52], but depends on the temperature at which it was processed. The same sample processed at a lower temperature had an indentation modulus of around 320 GPa, which is consistent with values found in other published works[52,53]. The results from the finite element simulations appear to be more consistent with the published literature than those from the analytical solutions. Even when considering the minimum indentation modulus from the range calculated analytically, there is a difference of nearly 120 GPa between the analytical result and the lower published value for indentation modulus of tungsten using cubic elastic constants. The range indentation moduli of tungsten found using tetragonal elastic constant matches the published values well. Ultimately, there is some uncertainty in these results because of the lack of research in this area. Indentation modulus is not widely published for tungsten or for its alloys, particularly rhenium alloys, therefore, it is difficult to ensure the accuracy of these results other than by checking the accuracy of the methods with different, more researched materials.

In addition, there is a lack of published work for the elastic constants of both irradiated tungsten and irradiated tungsten-rhenium. Therefore, it was not possible to analyze the indentation modulus of tungsten or tungsten-rhenium post-radiation exposure to compare this information with the virgin materials. While this lack of information indicates the significance of this work, more experimental data is needed to perform an accurate and useful comparison.

4.3 Limitations and Benefits of the Methodology

As with other data analysis methods, the limitations and benefits must be considered to understand how to most effectively use finite element models. Understanding and comparing

results obtained from finite element simulations allows these benefits and limitations to be considered. FEA is limited because of the parameter knowledge required before running simulations. Figure 16 below shows a comparison between nanoindentation and simulation results from spherical indentation of Ni-Co. While the force-displacement graph shows strong agreement between the experimental and simulation curves, the profile of indention in the material differs significantly. Without exact knowledge of the indenter geometry, studies performing FEA may falsely assume indenter tips to be defect-free (see Fig. 16b)[33].

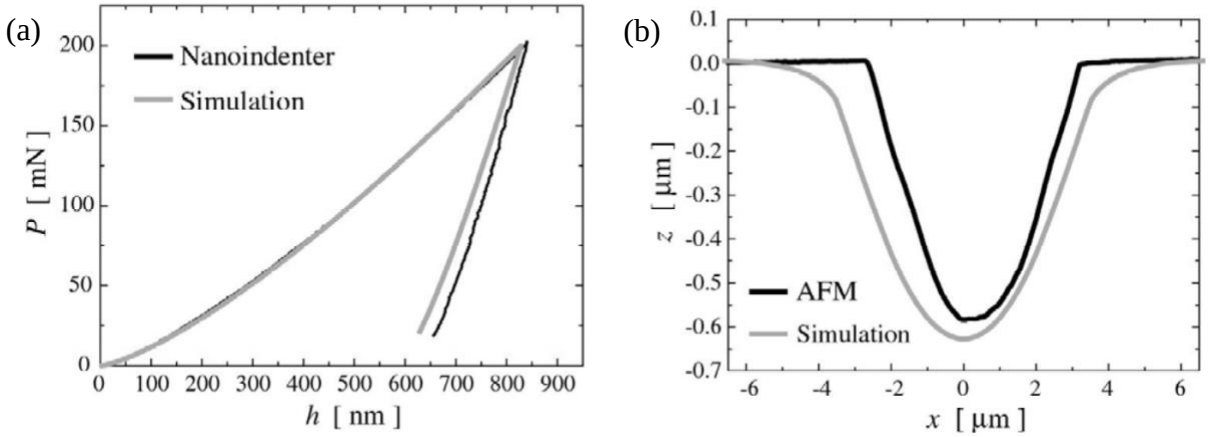

Figure 16. (a) Force-penetration curve and (b) indention profile comparison for spherical nanoindentation and FEA simulation of Ni-Co[33].

Many studies employing FEA used reverse analysis to determine significant parameters of the simulation[28,33,54]. This process combined with the additional knowledge provided by FEA as compared to nanoindentation has aided in findings of the significance of indenter tip bluntness[55]. As previously discussed, indenter sharpness is necessary parameter to consider when performing finite element simulations. Surface conditions and defects of the indenter tip have a significant impact on the force-displacement data gathered at indentation depths of 20 nm or less[54]. Of these

defects, the bluntness of the tip, specifically its radius was found to be the most significant parameter to achieve FEA simulations that agree with experimental data[54]. Figure 17 shows a diagram of this bluntness radius, a.

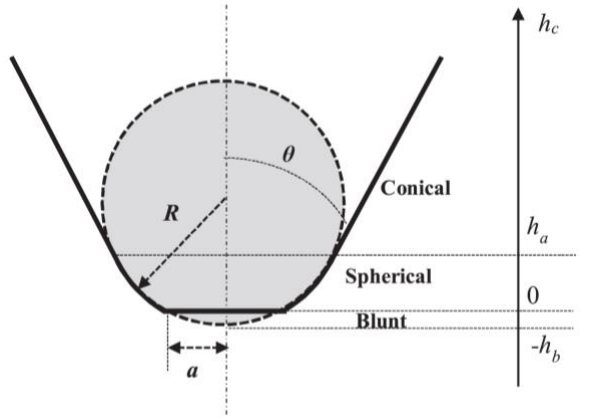

Figure 17. Conical spherical indenter with blunt tip of radius, a, considered[54].

Using reverse analysis, various bluntness radii were considered to determine the radius that best fit the experimental data for the indentation tip used, as shown in Fig. 18 below.

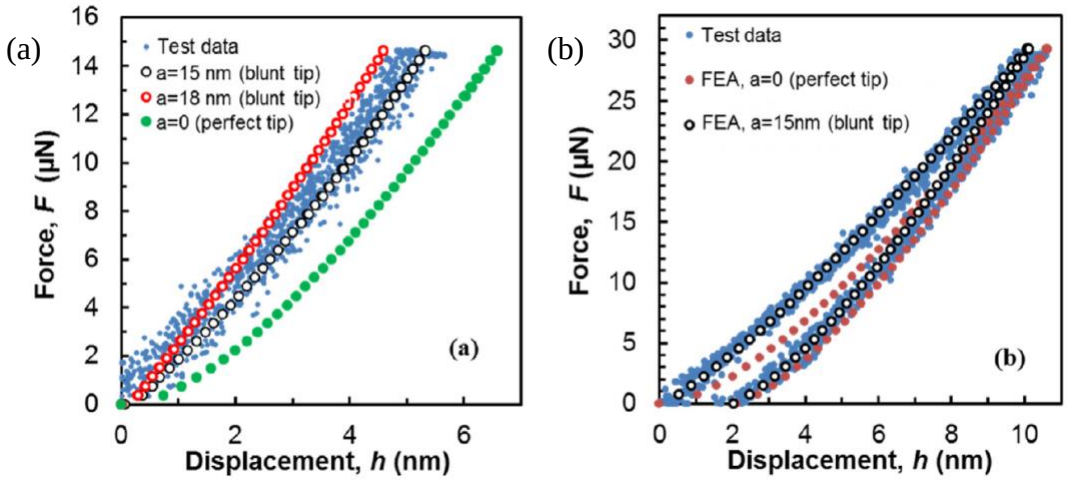

Figure 18. Comparing experimental and simulation results (a) to determine the radius of bluntness and (b) to examine the difference between a perfectly sharp and blunt tip[54].

Finite element analysis is beneficial because it allows for the collection of data about stress and strain fields directly under indenter tips[26]. Studies have used information about plastic strain from FEM to determine which part(s) of the sample experienced significant amounts of strain[28]. Using FEM, strain and deformation can be analyzed during both loading and unloading stages of the indentation without interrupting the constant loading process.

Although elastic tensors of a material vary with temperature, there is relatively little uncertainty in their calculation[56]. Because the Python simulation calculates modulus directly from elastic constants, it should not produce a large variation of the indentation modulus. However, the simulation has been coded to provide a range of acceptable indentation values based on the elastic tensors to incorporate attempted uncertainty quantification in experimental data. Two sources of uncertainty exist, aleatoric and epistemic, both of which were considered in the creation of the range of indentation moduli. Aleatoric uncertainty, or uncertainty caused by natural randomness, must be accounted for in all experiments. Epistemic uncertainty, or uncertainty in the model, may be caused by inaccurate measurements, limited data or a small sample size, or even limited knowledge of the subject. Literature has suggested that the most significant source of error and uncertainty in experiments concerning elastic tensors is experimental measurement error[56]. With the output of indentation modulus given as a range of acceptable values, researchers may use the Python simulation in conjunction with their research to verify their results. The variability of elastic modulus of a material depends on the nature of the material; because tungsten is a metal, the variability of its elastic modulus is expected to be within 6 – 10%[57]. Because the elastic tensors were used as an input for both the finite element simulations and the analytical solution, the uncertainty that exists for the elastic tensors reflect the uncertainty in the results of both.

4.4 Future Work

It is critical to understand the impact of irradiation on a substance's material and mechanical properties. Through a survey of current literature, it has been determined that a synthesis of methods is the most effective way to acquire accurate, repeatable data about such properties. No single method is able to provide whole and perfect results; therefore, a combination of methods is able to ensure complete and accurate data. This synthesis includes the use of both Berkovich and spherical nanoindenter tips, as well as both experimental indentations and analytical simulations.

Future work for this study aims to perform more extensive and varied finite element simulations. As discussed, the lack of published data on the elastic constants of irradiated tungsten and tungsten-rhenium prevented simulations from being performed on such materials to analyze indentation moduli. However, as such information becomes available, the techniques discussed may be performed. In addition to expanding the type of materials, several aspects of the finite element simulations may be varied in future research. Instead of a spherical nanoindenter, a Berkovich indenter may be simulated. With a Berkovich indenter, the radius of the indenter tip may be varied to investigate the impact. Finally, the contact between the indenter and the material being indented may be analyzed by incorporating different friction coefficients to determine the impact of friction on the simulation. Several studies cited in this work have performed similar tests on nanoindentation experiments and simulations of materials other than tungsten, so a comparison to these works would be of interest.

References

1. Pathak, S. *et al.* Probing nanoscale damage gradients in ion-irradiated metals using spherical nanoindentation. *Sci. Rep.* (2017). doi:10.1038/s41598-017-12071-6
2. Patra, A. & McDowell, D. L. Crystal plasticity-based constitutive modelling of irradiated bcc structures. *Philos. Mag.* **92,** 861–887 (2012).
3. Gilbert, M. R. & Sublet, J. C. Neutron-induced transmutation effects in W and W-alloys in a fusion environment. *Nucl. Fusion* **51,** (2011).
4. Saleh, M. *et al.* Relationship between damage and hardness profiles in ion irradiated SS316 using nanoindentation - Experiments and modelling. *Int. J. Plast.* **86,** 151–169 (2016).
5. Armstrong, D. E. J. *et al.* Small-scale characterisation of irradiated nuclear materials: Part II nanoindentation and micro-cantilever testing of ion irradiated nuclear materials. *J. Nucl. Mater.* **462,** 374–381 (2015).
6. Khan, A. *et al.* Effect of rhenium irradiations on the mechanical properties of tungsten for nuclear fusion applications. *J. Nucl. Mater.* **477,** 42–49 (2016).
7. Fowler, J. M. *Energy and the Environment*. (McGraw-Hill, 1975).
8. Mary, B. Y., Griggs, B., By, P. & Voorhes, T. H. E. Why Can't We Decide What To Do About Nuclear Energy ?
9. US Energy Information Administration. What is U.S. electricity generation by energy source? (2018). Available at: https://www.eia.gov/tools/faqs/faq.php?id=427&t=21. (Accessed: 2nd April 2018)
10. United States Nuclear Regulatory Commision. Map of Power Reactor Sites. (2017). Available at: https://www.nrc.gov/reactors/operating/map-power-reactors.html. (Accessed: 4th April 2018)
11. Nero Jr., A. V. *A Guidebook to Nuclear Reactors*. (Berkeley : University of California Press, 1979).
12. Murphy, A. W. *The Nuclear Power Controversy*. (Prentice-Hall, 1976).
13. Mettler, F. A., Huda, W., Yoshizumi, T. T. & Mahesh, M. Effective Doses in Radiology and Diagnostic Nuclear Medicine: A Catalog. *Radiology* **248,** 254–263 (2008).
14. AJ Software and Multimedia. Nuclear Fission: Basics. Available at: http://www.atomicarchive.com/Fission/Fission1.shtml. (Accessed: 2nd May 2018)
15. Ciupiński *et al.* TEM observations of radiation damage in tungsten irradiated by 20 MeV W ions. *Nucl. Instruments Methods Phys. Res. Sect. B Beam Interact. with Mater. Atoms* **317,** 159–164 (2013).
16. Bushby, A. J., Roberts, S. G. & Hardie, C. D. Nanoindentation investigation of ion-irradiated Fe-Cr alloys using spherical indenters. *J. Mater. Res.* **27,** 85–90 (2012).
17. Kiener, D., Hosemann, P., Maloy, S. A. & Minor, A. M. In situ nanocompression testing of irradiated copper. *Nat. Mater.* **10,** 608–613 (2011).
18. Weaver, J. S. *et al.* Spherical nanoindentation of proton irradiated 304 stainless steel: A comparison of small scale mechanical test techniques for measuring irradiation hardening. *J. Nucl. Mater.* **493,** 368–379 (2017).
19. Fukuda, M., Yabuuchi, K., Nogami, S., Hasegawa, A. & Tanaka, T. Microstructural development of tungsten and tungsten-rhenium alloys due to neutron irradiation in HFIR. *J. Nucl. Mater.* **455,** 460–463 (2014).
20. He, J. C., Tang, G. Y., Hasegawa, A. & Abe, K. Microstructural development and

irradiation hardening of W and W-(3-26) wt%Re alloys after high-temperature neutron irradiation to 0.15 dpa. *Nucl. Fusion* **46,** 877–883 (2006).
21. World Nuclear Association. Nuclear Power Reactors. (2018). Available at: http://www.world-nuclear.org/information-library/nuclear-fuel-cycle/nuclear-power-reactors/nuclear-power-reactors.aspx. (Accessed: 3rd April 2018)
22. Hasegawa, A., Tanno, T., Nogami, S. & Satou, M. Property change mechanism in tungsten under neutron irradiation in various reactors. *J. Nucl. Mater.* **417,** 491–494 (2011).
23. Barabash, V., Federici, G. & Rödig, M. Neutron irradiation effects on plasma facing materials. *J. Nucl. Mater.* **283–287,** 138–146 (2000).
24. Hosemann, P., Kiener, D., Wang, Y. & Maloy, S. A. Issues to consider using nano indentation on shallow ion beam irradiated materials. *J. Nucl. Mater.* **425,** 136–139 (2012).
25. Gibson, J., Armstrong, D. & Roberts, S. The micro-mechanical properties of ion irradiated tungsten. *Phys. Scr.* **T159,** (2014).
26. Karimzadeh, A., Ayatollahi, M. R. & Alizadeh, M. Finite element simulation of nano-indentation experiment on aluminum 1100. *Comput. Mater. Sci.* **81,** 595–600 (2014).
27. Weaver, J. S. & Kalidindi, S. R. Mechanical characterization of Ti-6Al-4V titanium alloy at multiple length scales using spherical indentation stress-strain measurements. *Mater. Des.* (2016). doi:10.1016/j.matdes.2016.09.016
28. Dao, M., Chollacoop, N., Vliet, K. J. Van, Venkatesh, T. a & Suresh, S. Computational modeling of the forward and reverse problems. *instrumented sharp indentation, Acta Mater.* **49,** 3899–3918 (2001).
29. Pethicai, J. B., Hutchings, R. & Oliver, W. C. Hardness measurement at penetration depths as small as 20 nm. *Philos. Mag. A* **48,** 593–606 (1983).
30. Weaver, J. S., Priddy, M. W., McDowell, D. L. & Kalidindi, S. R. On capturing the grain-scale elastic and plastic anisotropy of alpha-Ti with spherical nanoindentation and electron back-scattered diffraction. *Acta Mater.* (2016). doi:10.1016/j.actamat.2016.06.053
31. Basu, S., Moseson, A. & Barsoum, M. W. On the determination of spherical nanoindentation stress-strain curves. *J. Mater. Res.* **21,** 2628–2637 (2006).
32. He, L. H., Fujisawa, N. & Swain, M. V. Elastic modulus and stress-strain response of human enamel by nano-indentation. *Biomaterials* **27,** 4388–4398 (2006).
33. Stauss, S. *et al.* Determining the stress – strain behaviour of small devices by nanoindentation in combination with inverse methods. *Microelectron. Eng.* **68,** 818–825 (2003).
34. Bhattacharya, A. K. & Nix, W. D. Finite element simulation of indentation experiments. *Int. J. Solids Struct.* **24,** 881–891 (1988).
35. Doerner, M. F. & Nix, W. D. A method for interpreting the data from depth-sensing indentation instruments. *J. Mater. Res.* **1,** 601–609 (1986).
36. Loftness, R. L. *Nuclear power plants : design, operating experience, and economics.* (Princeton, N.J. : Van Nostrand, [1964], 1964).
37. Lai, C., Wang, J., Zhou, F., Liu, W. & Miao, N. Reduction, sintering and mechanical properties of rhenium-tungsten compounds. *J. Alloys Compd.* **735,** 2685–2693 (2018).
38. Klimenkov, M. *et al.* Effect of neutron irradiation on the microstructure of tungsten. *Nucl. Mater. Energy* **9,** 480–483 (2016).
39. Ueda, Y. *et al.* Recent progress of tungsten R&D for fusion application in Japan. *Phys.*

Scr. T **T145,** (2011).
40. Patel, D. K. & Kalidindi, S. R. Correlation of spherical nanoindentation stress-strain curves to simple compression stress-strain curves for elastic-plastic isotropic materials using finite element models. *Acta Mater.* **112,** 295–302 (2016).
41. Lichinchi, M., Lenardi, C., Haupt, J. & Vitali, R. Simulation of Berkovich nanoindentation experiments on thin films using finite element method. *Thin Solid Films* **333,** 278–286 (1998).
42. Bhattacharya, A. K. & Nix, W. D. Finite element analysis of cone indentation. *Int. J. Solids Struct.* **27,** 1047–1058 (1991).
43. Somekawa, H. & Schuh, C. A. Effect of Crystal Orientation on Nanoindentation Behavior in Magnesium. *Metall. Mater. Trans. A* **47,** 3227–3234 (2016).
44. Esqué-De Los Ojos, D., Očenášek, J. & Alcalá, J. Sharp indentation crystal plasticity finite element simulations: Assessment of crystallographic anisotropy effects on the mechanical response of thin fcc single crystalline films. *Comput. Mater. Sci.* **86,** 186–192 (2014).
45. Pang, K. H., Tymicki, E. & Roy, A. Investigations and finite element analysis. **000,** 1–7 (2017).
46. Casals, O. & Forest, S. Finite element crystal plasticity analysis of spherical indentation in bulk single crystals and coatings. *Comput. Mater. Sci.* **45,** 774–782 (2009).
47. Franzoso, G. Elastic Anisotropy of Lamellar Bone Measured by Nanoindentation. *Dr. thesis* 128 (2009). doi:10.1115/1.3005162
48. Lowrie, R. & Gonas, A. M. Single-crystal elastic properties of tungsten from 24°to 1800°C. *J. Appl. Phys.* **38,** 4505–4509 (1967).
49. Materna, A., Haušild, P. & Nohava, J. A numerical investigation of the effect of cubic crystals orientation on the indentation modulus. *Acta Phys. Pol. A* **128,** 693–696 (2015).
50. Bonny, G., Bakaev, A., Terentyev, D. & Mastrikov, Y. A. Elastic properties of the sigma W-Re phase: A first principles investigation. *Scr. Mater.* **128,** 45–48 (2017).
51. Wei, N. *et al.* First-principles study of the phase stability and the mechanical properties of W-Ta and W-Re alloys. *AIP Adv.* **4,** (2014).
52. Iveković, A., Galatanu, A. & Novak, S. Low-activation W-Si-C composites for fusion application. *Fusion Eng. Des.* **100,** 638–645 (2015).
53. Barbato, G. *et al.* CIRP Annals - Manufacturing Technology Uncertainty evaluation of indentation modulus in the nano-range : Contact stiffness contribution. *CIRP Ann. - Manuf. Technol.* **66,** 495–498 (2017).
54. Zhang, Y., Wang, H., Li, X., Tang, H. & Polycarpou, A. A. A finite element correction method for sub-20 nm nanoindentation considering tip bluntness. *Int. J. Solids Struct.* **129,** 49–60 (2017).
55. Zhang, J., Niebur, G. L. & Ã, T. C. O. Mechanical property determination of bone through nano- and micro-indentation testing and finite element simulation. **41,** 267–275 (2008).
56. Ledbetter, H. M., Frederick, N. V. & Austin, M. W. Elastic-constant variability in stainless-steel 304. *J. Appl. Phys.* **51,** 305–309 (1980).
57. Sawa, T. & Tanaka, K. Evaluating Performance of Nanoindentation Instruments. *J. Mater. Res.* **16,** 3084–3096 (2001).